Shock Analysis of E-Glass/Epoxy Composite Submersible Hull Subjected to Pressure Loads of Underwater Explosion using Finite Element Method - Experimental Validation

A. Chennakesava Reddy

Abstract— Underwater explosion is a most important peril to ships and submarines, given that detonation underneath a hull can produce greater damage than an above-surface one of the same explosive size. In this paper, an attempt has been made to predict the influence of shock pressure loading on the submersible hull using finite element analysis. The maximum displacement of the submerged hull has been found to be 0.0712 m for the explosion charge weight of 25 kg. The damage has occurred in the submersible hull exposed to explosion charge weight of 25 kg. The impact test by falling weight results were in good agreement with the results obtained through finite element analysis. The hull damage can be endorsed due to failure of fibers in tension and the failure of matrix in shear.

Index Terms— Submersible hull, shock pressure load, finite element analysis, impact test by falling weight, E-glass/epoxy composite.

1. INTRODUCTION

UNDERWATER explosions are very critical and multifaceted problems for naval surface ships or submarines, since detonations near a ship can damage the vessel. The design of submersible hull and the estimation of damage are practically complex involving material and geometric nonliniearities. Composite materials are being used in a variety of structures because of their specific properties. Modern underwater vehicles are a good example: they are light, sturdy and corrosion resistant. The demands posed on such structures are good sailing properties, good maneuverability and the ability to withstand designed pressure.

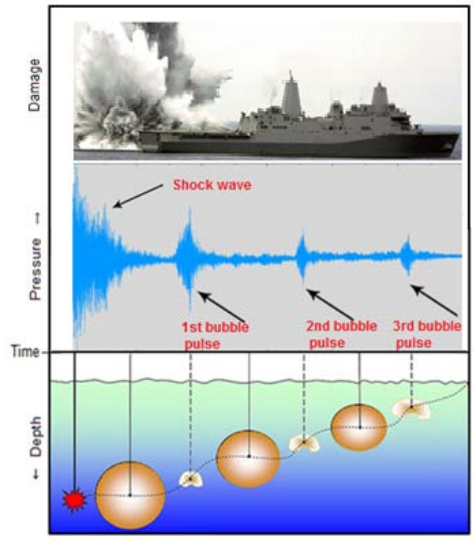

Fig. 1. Pressure waves and bubble phenomena of underwater explosion.

Because the explosion process occurs rapidly, it abruptly increases the pressure, which in turn compresses the surrounding fluid medium. This compression propagates in the radial direction as a shock wave. Simultaneously, the gas bubbles formed by the gaseous products of the explosion expand in the radial direction at relatively slow as compared to shock wave. This gas bubbles can expand till the hydrostatic pressure exceeds the internal gas pressure. At this phase, the gas bubbles contract. During this short interval, another compression wave is created in the surrounding medium. This process of contraction and expansion is repeated till low intensity pulses are generated (figure 1). The process of expansion and contraction repeats throughout the duration of the gas bubble, making it an oscillating system. Figure 2 illustrates this and is a result of energy loss during the oscillation process. In addition to the said phenomena, the gas bubbles tend to migrate upwards because of gravity. The migrated gas bubbles burst at the water surface generating spray dome, plume and explosion generated water waves.

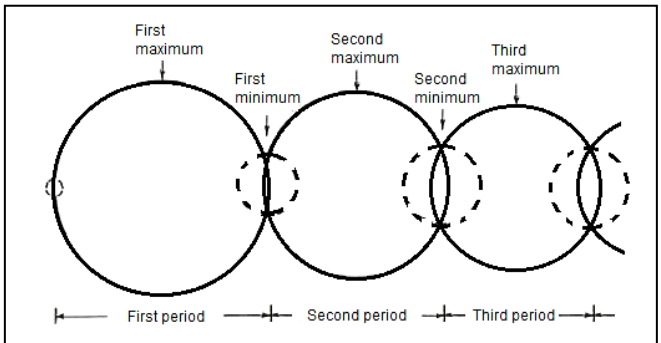

Fig. 2. Oscillation of bubble.

The Australian Navy conducted an underwater explosion test on one of its ships. The test consisted of a MK 48 torpedo detonated under the keel of the ship. Figure 3 shows

• *A. Chennakesava Reddy is currently Proffsor and BOS Chairman, Department of Mechanical engineering, JNT University Hyderabad, India, Mobile-09440568776. E-mail: acreddy@jntuh.ac.in*

the sequence of events of the under keel torpedo test. The under explosion lifts the ship's hull out of the water in a hogging motion and then crashing down in a sagging motion and ultimately breaking the ship in half. The shock-wave and the gaseous bubble generated by the underwater explosion both contributed to the damage of the ship.

Fig. 3. Illustration of Australian Navy MK 46 Torpedo Test (Courtesy: [1]).

Huang and Kiddy [2] studied the transient interaction of a spherical shell with an underwater explosion shock wave and subsequent pulsating bubble, based on their approach on the finite element method coupled with the Eulerian–Lagrangian method. According to their results, the structural response, as well as interactions among the initial shock wave, the structure, its surrounding media and the explosion bubble must be considered. Kwon and Fox [3] applied numerical and experimental techniques to investigate the nonlinear dynamic response of a cylinder subjected to a side-on, far-field underwater explosion. Comparisons between the strain gage measurements and the numerical results at different locations revealed a good agreement. Shin and Chisum [4] employed a coupled Lagrangian–Eulerian finite element analysis technique as a basis to investigate the response of an infinite cylindrical and a spherical shell subjected to a plane acoustic step wave. Santiago et al. [5] presented a comparison between the finite element transient response of a thin walled aluminum cylinder subjected to blast loads with experimental results in which the strains were measured. Jiang and Olson [6] conducted the finite element approach for predicting the nonlinear behavior of isotropic and stiffened cylindrical shells under air blast loads. Gong and Lam [7] found that the stiffeners could increase the circumferential strength of the composite submersible hull.

Fiberglass is a strong lightweight material and is used for many products. Its bulk strength and weight are also better than many metals, and it can be more readily molded into complex shapes [8]. Applications of fiberglass include aircraft, boats, automobiles, hot tubs, water tanks, etc.

Epoxy resins are formed by a reaction of an epoxide (like epichlorohydrin) with a hardener or polyamine (like triethylenetetramine) that has tremendous cross-linking to create a very tough and yet stiff polymer. The viscosity of epoxies is another step higher than polyesters or vinyl esters. Most epoxies start in the range of 900 centipoise. Epoxies generally out-perform most other resin types in terms of mechanical properties and resistance to environmental degradation, which leads to their almost exclusive use in aircraft components. As a laminating resin their increased adhesive properties and resistance to water degradation make these resins ideal for use in applications such as boat building. Here, epoxies are widely used as a primary construction material for high-performance boats or as a secondary application to sheath a hull or replace water-degraded polyester resins and gel coats [9], [10], [11].

The present work was realized to select the most suitable shape and material to withstand pressure loads of underwater explosion. In the current study, E-glass fiber/epoxy composite was used for the cylindrical submersible hull. Non-linear finite element analysis was employed to estimate the influence of shock pressure loading on the structure of submersible hull. An attempt was made to correlate the simulation results with those acquired by the impact test by falling weight.

2. THEORETICAL BACKGROUND

The theoretical background of underwater explosion and finite element modeling are discussed.

2.1 Shock Wave Pressure

The underwater shock wave generated by the explosion is superimposed on the hydrostatic pressure. The pressure history $P(t)$ of the shock wave at a fixed location starts with an instantaneous pressure increase to a peak P_{max} followed by a decline which initially is usually approximated by an exponential function. Thus, according to the empirical equation of Cole [12]:

$$P(t) = P_o e^{-t/\theta} \quad 0 \ll t \ll \theta \tag{1}$$

The peak pressure (P_o) and the decay constant (θ) are given by

$$P_o = 52.16 \times 10^6 \left(W^{1/3}/R\right)^{1.13} \tag{2}$$

$$\theta = 92.5 \times W^{1/3} \left(W^{1/3}/R\right)^{-0.22} \tag{3}$$

where W is the charge weight (kg) and R is the stand-off distance (m).

Because of the spherical spreading nature of the shock wave, the wave reaches different locations at different times, i.e. there is time delay. The time delay (t_d) can be calculated using the radial distance at any location (R), the shortest radial distance (R_o) and the sound wave velocity (c), as follows:

$$t_d = (R - R_o)/c \tag{4}$$

By incorporating the time delay, Eq. (1) is rewritten in the following form:

$$P(t) = P_o e^{-(t-t_d)/\theta} \quad 0 \ll t \ll \theta \tag{5}$$

2.2 Shock Wave Velocity

As the wave travels from the explosion, the profile of the shock wave broadens and the amplitude reduces as shown in figure 2. The velocity in the vicinity of the explosion depends on the peak pressure of the shock wave and the acoustic velocity, as given by

$$c_s = c_a \times (1 + 6 \times 10^{-10} P_o) \tag{6}$$

As the shock wave propagates, it sets the water particle

in the vicinity in motion. The water particle velocity associated with the shock wave is given by

$$v(t) = P(t)/\rho c \quad (7)$$

where ρ is the density of the fluid medium.

The maximum radius (R_{max}) during the first pulsation and the duration (T) of the first pulsation are given by

$$R_{max} = 3.3 \times (W/Z_o)^{1/3} \quad (8)$$

$$T = 2.06 \times \left(W^{1/3}/{Z_o}^{5/6}\right) \quad (9)$$

$$Z_o = D + 10 \quad (10)$$

where, D is water depth, Z_o is the reference depth.

2.3 Secondary Shock Wave

During the contraction phase of the gas bubble oscillation, when the bubble reaches its minimum, a pressure pulse known as the secondary shock wave, of small amplitude is emitted. The peak pressure of the secondary pressure pulse is given by

$$P_2 = 2590 \times \left(W^{1/3}/R\right) \quad (11)$$

2.4 Gas Bubble Migration

When the gas bubble has last buoyancy, the migration of gas bubble occurs. The migration of the gas bubble from the location of the explosive charge up to the location corresponding to the first bubble pulse is given by

$$m = (90/Z_o)W^{1/2} \quad (12)$$

Since a ship can be subjected to a large variety of underwater explosion (variation in charge weight, standoff distance), the relation between attack severity and geometry must be determined. For damage predictions for submarines, this factor is referred to as the Hull Shock Factor (HSF). It has been found that

$$\text{HSF} = \sqrt{W}/R \quad (13)$$

where, W is the charge weight and R is the standoff distance.

2.5 Finite Element Modeling

For a fully or partially submerged structure subjected to an underwater shock wave, the structure may exhibit material and geometrical nonlinear behavior. Based on the theorem of virtual displacement, the governing equation [13] of the problem can be expressed in matrix as given below:

$$[M_s]\{\ddot{u}\} + [C_s]\{\dot{u}\} + [K_s]\{u\} = \{f\} \quad (14)$$

where,

$[M_s] = \int \rho_s [N]^T [N] dv, [C_s] = \int \rho_s \alpha_c [N]^T [N] dv,$
$[K_s] = \int [B]^T [D][B] dv$ and $\{f\} = \int [N]^T f dv$

$[M_s]$, $[C_s]$ and $[K_s]$ are the structural mass, damping and stiffness matrices, respectively. $[N]$, $[B]$ and $[D]$ are the shape function, strain matrix and matrix of elastic-plastic tangent stiffness, respectively. $\{u\}$ and $\{f\}$ are the structural displacement and the external force vector, respectively.

For a structure submerged in an infinite acoustic medium, the governing equation of the wet surface of the shell is based on the Doubly Asymptotic Approximation as given below:

$$[M_f]\{\ddot{P}_s\} + \rho_f c[A_f]\{\dot{P}_s\} + \rho_f c[\varphi_f][A_f]\{P_f\} = \rho_f c[M_f]\{\dot{v}_s\} + [\varphi_f][M_f]\{v_s\} \quad (15)$$

where,

$$[\varphi_f] = \alpha \rho_f c[A_f][M_f]^{-1} \quad (16)$$

$[M_f]$ is the symmetric fluid mass matrix a is the scale parameter bounded $0 \ll \alpha \ll 1$, ρ_f and c are the fluid density and sound velocity, respectively. $\{v_s\}$ is the vector of scattered-wave fluid particle velocities normal to the structural surface.

The fluid surface is coupled to the structural response by the following equation

$$\{v_s\} = [G]^T\{\dot{u}\} - \{v_i\} \quad (17)$$

where $\{v_i\}$ is the fluid incident velocity.

2.6 Tsai-Hill Criterion

Other treatments that take into account the interactions between failure modes are mostly based on modifications of yield criteria for metals. The most important of these is the Tsai-Hill Criterion, which is an adaptation of the von Mises Criterion.

von Mises Criterion for Metals:

$$(\sigma_1 - \sigma_2)^2 + (\sigma_2 - \sigma_3)^2 + (\sigma_3 - \sigma_1)^2 = 2\sigma_y{}^2 \quad (18)$$

where σy is the metal yield stress.

For in-plane stress states (σ3 = 0) this reduces to

$$\left(\frac{\sigma_1}{\sigma_y}\right)^2 + \left(\frac{\sigma_2}{\sigma_y}\right)^2 - \frac{\sigma_1\sigma_2}{\sigma_y{}^2} = 1 \quad (19)$$

This is then modified to take into account the anisotropy of composites and the different failure mechanisms to give the following expression.

$$\left(\frac{\sigma_1}{\sigma_{1y}}\right)^2 + \left(\frac{\sigma_2}{\sigma_{2y}}\right)^2 - \frac{\sigma_1\sigma_2}{\sigma_{1y}{}^2} - \frac{\sigma_1\sigma_2}{\sigma_{2y}{}^2} + \frac{\sigma_1\sigma_2}{\sigma_{3y}{}^2} + \left(\frac{\tau_1}{\tau_{12y}}\right)^2 = 1 \quad (20)$$

The metal yield stresses can be regarded as composite failure stresses and since composites are transversely isotropic (σ2u = σ3u) we arrive at the Tsai-Hill Criterion for composites.

$$\left(\frac{\sigma_1}{\sigma_{1y}}\right)^2 + \left(\frac{\sigma_2}{\sigma_{2y}}\right)^2 - \frac{\sigma_1\sigma_2}{\sigma_{1y}{}^2} + \left(\frac{\tau_1}{\tau_{12y}}\right)^2 = 1 \quad (21)$$

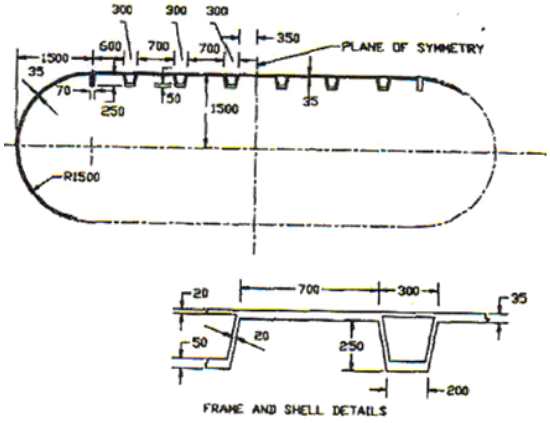

Fig. 4. Physical model of submersible hull.

3. Material and Methods

The physical model of a submersible hull is shown figure 4. The major dimensions of the submersible hull are as follows:

Diameter = 3 m
Length = 9.5 m
Thickness = 0.035 m

The finite element analysis of the submersible hull was carried out using DYTRAN non-linear finite element code. For the finite element analysis, the explosion, fluid and submersible hull were modeled as an integral unit. The fluid and explosion were meshed with 8 node Eulerian solid element (figure 5a). The number of elements was 106160. The fluid domain of 5 m width in transverse direction and 3 m width in the longitudinal direction from the submersible hull was considered for modeling. The submersible hull was discretized with 4 node Lagrangian element (figure 5b). The number of elements was 7708. The explosion and fluid were interfaced using an Eulerian-Eulerian coupling. The fluid and the submersible hull were interfaced using Lagrangian-Eulerian coupling. In the present investigation, the explosion was assumed on the normal line passing through the centerline of the submersible hull at a distance of 5 m. The exploded charge weight was varied from 1kg to 25 kg.

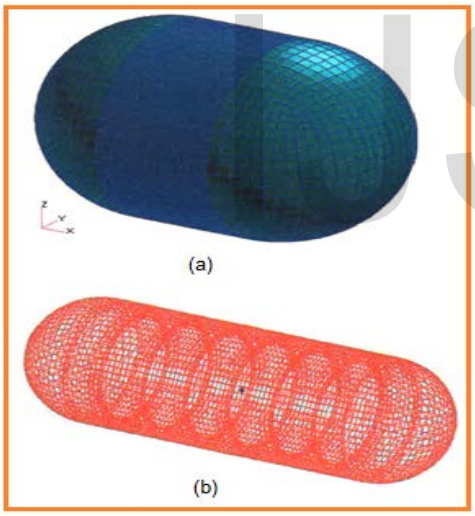

Fig. 5. Finite element modeling (a) fluid domain and explosion and (b) submersible hull.

3.1 Modelling and Analysis

For the finite element analysis, the fluid was modeled using Eulerian solid element with Tait's equation of state and the explosion was modeled using Eulerian solid element with JWL equation of state. The material constants used in the Tait's equation of state are as follows:

$\rho = 1025\ kg/m^3$
$a = 48402.7105\ Pa$
$b = 3.01E8$ Pa
$R = 7.15$
$C_0 = 1450\ m/s$

The equation of state from Jones-Wilkins-Lee (JWL) is used to describe the detonation products of explosives.

$$p = A\left(1 - \frac{\omega}{R_1 V}\right)\exp(-R_1.V) + B\left(1 - \frac{\omega}{R_2 V}\right)\exp(-R_{12}.V) + \frac{\omega e_0}{V} \quad (22)$$

The ratio $V = \rho_e/\rho$ is defined by using ρ_e is the density of explosive (solid part) and ρ is the density of detonation products. The parameters A, B, R_1, R_2 and ω are given below:

$\rho = 1610\ kg/m^3$
$A = 371.2\ GPa$
$B = 3.2306\ GPa$
$R_1 = 4.15$
$R_2 = 0.95$
$\omega = 0.3$

The composite submersible hull was made of glass fiber reinforced plastic. The material properties for the cylindrical section are given below:

$E_{11} = 24.177\ GPa$
$E_{22} = 36.747\ GPa$
$v_{21} = v_{12} = 0.1246$
$G_{12} = 9.955\ GPa$
$\sigma_{tx} = \sigma_{tv} = 210\ MPa$
$\sigma_{cx} = \sigma_{cv} = 690\ MPa$
$\rho = 2028\ kg/m^3$
$\tau = 106\ MPa$

The material properties for the hemispherical end-closures are given below:

$E_{11} = E_{22} = 25.065\ GPa$
$v_{21} = v_{12} = 0.259$
$G_{12} = 9.955\ GPa$
$\sigma_{tx} = \sigma_{tv} = 210\ MPa$
$\sigma_{cx} = \sigma_{cv} = 690\ MPa$
$\rho = 2028\ kg/m^3$
$\tau = 106\ MPa$

The analysis of the coupled field problem was solved using explicit integration scheme. Three incremental time steps of 0.05, 0.1 and 0.2 microseconds were used for the analysis. The explosion and fluid were interfaced using Eulerian-Eulerian coupling and the fluid and shell were interfaced using arbitrary Lagrangian-Eulerian coupling. The initial conditions used in the explosion were specific internal energy (4.16 x 10^6 K/kg) and detonation velocity (6730 m/s). The explosive element was modeled using eight node Eulerian solid elements. The element length was 0.426 m. The stand-off distance was 5 m.

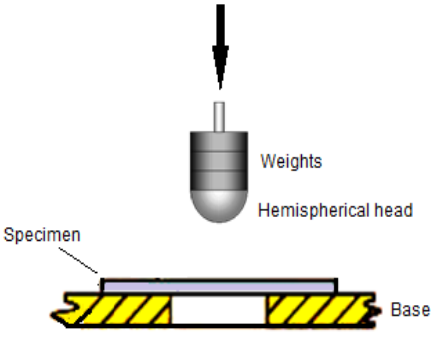

Fig. 6. Impact testing by falling weight

3.2 Impact Test by Falling Weight

The impact test was performed using an instrumented falling weight testing machine with no energy storage device: the maximum impact energy is limited by the adjustable falling height and the fixed mass, 10 kg, of the impactor. The impactor mass together with the height of drop determines the energy of impact. With an increase in mass and height the potential energy of the dart will increase and thus on releasing the tool holding assembly the potential energy is converted to kinetic energy. Falling weight impact test setup is shown in figure 6. The dart material used was steel. In accordance with ASTM D 3029 standard, a thin-square (150 mm side, 2 mm thick) specimen was employed.

4. Result and Discussion

The shock pressure loading of the fluid medium was applied on the surface of submersible hull through arbitrary Lagrangian-Eulerian coupling. The peak pressures were calculated for all the cases as given in table 1. The peak value was 36 MPa for a charge weight of 25 kg.

TABLE 1
Peak shock pressure loads

Charge weight (W), kg	Shock factor, $\sqrt{kg/m}$	Shock pressure, MPa
1	0.09	9
2	0.12	13
5	0.20	18
10	0.28	22
15	0.34	25
20	0.40	30
25	0.45	36

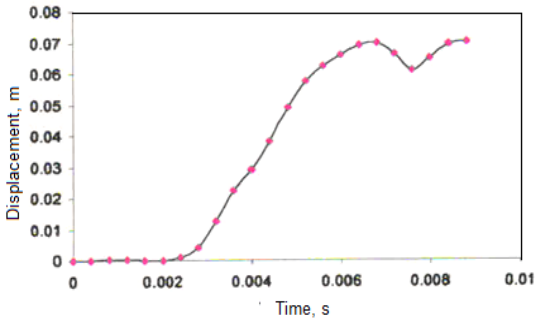

Fig. 7. Displacement-time history for charge weight of 25 kg.

4.1 Displacement -Time History

The displacement-time history of the submersible hull exposed to the explosion for a charge weight of 25 kg is shown in figure 7. The displacement increases with time until about 7 milliseconds and later it becomes oscillatory. The deformation of the submerged hull was obtained from the maximum displacement by subtracting the elastic deformation. The maximum displacement was 0.0712 m at 7 milliseconds. To emphasize the eloquence of results, the displacement contours are shown in figure 8. The plastic displacement was detected to be high on the submersible hull side exposed to the explosion (figure 8a). The elastic displacement was noticed on the back side (far away from the explosion) of the hull (figure 8b). Caldwell applied rigid plastic mechanism analysis to evaluate the ultimate strength of a ship's hull girder, and accounted for the effect of buckling by reducing the yield stress of the material at the buckled part. However, his method does not account for the post-collapse strength of the structural members which significantly influence the collapse strength. In fact, the present problem may be of hydroelasto-plasticity wherein the interaction between the fluid and structure must be considered. The severity of collapse can be expressed as the plastic deformation. The severity can be higher with larger waves in terms amplitude and height. The plastic deformation increases very rapidly and unstably after the ultimate strength is reached.

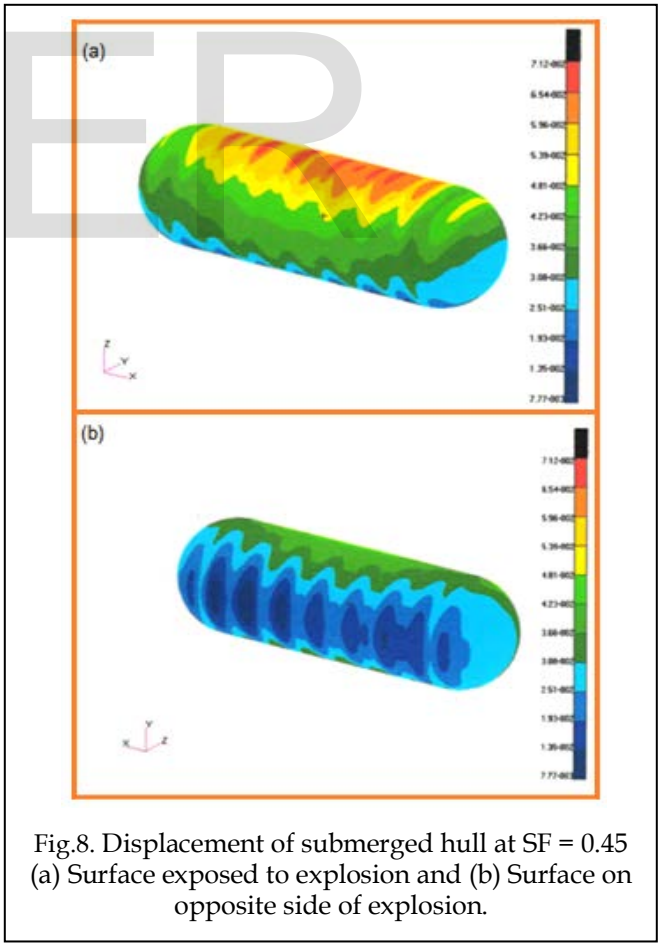

Fig.8. Displacement of submerged hull at SF = 0.45 (a) Surface exposed to explosion and (b) Surface on opposite side of explosion.

4.2 Stress -Time History

The tensile stress contours of the submersible hull subjected to for the explosion charge weight of 25 kg is shown in

figure 9. The maximum tensile stress along the longitudinal direction of the submersible hull was 212 MPa (figure 9a), while the maximum tensile stress along the circumferential direction of the submersible hull was 169 MPa (figure 9b). The maximum allowable tensile stress was 210 MPa. This indicates that the fibers fail along the longitudinal direction in tension. The compressive stress contours of the submersible hull subjected to for the explosion charge weight of 25 kg is shown in figure 10. The maximum compressive stress along the longitudinal direction of the submersible hull was 138 MPa (figure 10a), whereas the maximum compressive stress along the circumferential direction of the submersible hull was 146 MPa (figure 10b). The maximum allowable tensile stress was 690 MPa. The induced compressive stresses were less than the allowable compressive stress. The maximum shear stress was 108 MPa in the submersible hull (figure 11). Comparing this value with the allowable shear stress (106 MPa), the matrix fails in shear.

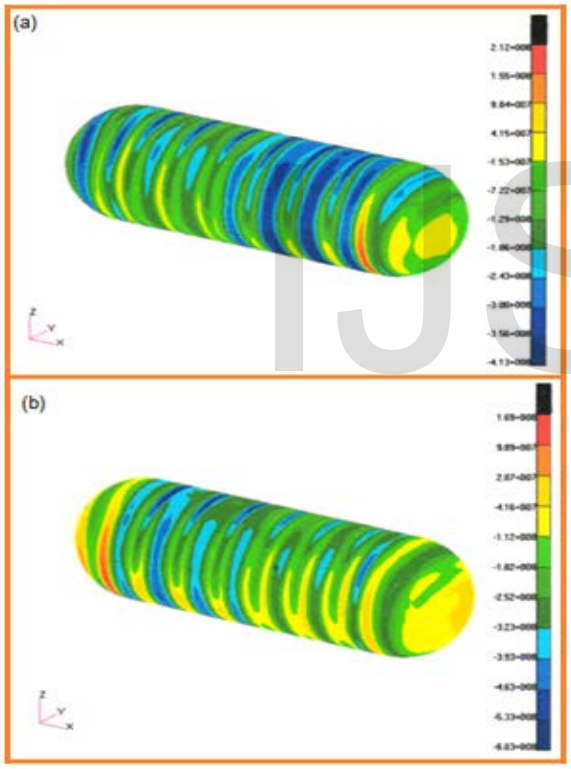

Fig. 9. Tensile stresses of submerged hull at SF = 0.45 (a) longitudinal and (b) circumferential.

When t = 0.0 sec, the shock wave has not yet contacted the hull and, thus, stresses and displacements are zero. When t = 0.004 sec (figure 12), the pressure hull is affected by the initial shock wave, inducing an elevating stress (350 MPa). When t = 0.007 sec, the stress concentrates on the side nearer to the explosion. When t = 0.009 sec, with the bubble pulsating wave passing through the hull, the stress reaches 212 MPa, causing the submersible hull to yield. Finally, at t = 0.01 sec, the stress becomes low and the next pulsating bubble wave comes into play. Al'tshuler, Novikov, and Divnov [14] summarized direct explosively-driven spallation experiments stating that "the resistance of metal to fracture in the case of a strong blow or explosion is not a constant characteristic of its strength, but rather may vary over a wide range depending on the pressure gradient (or on strain rate) in the interacting rarefaction waves".

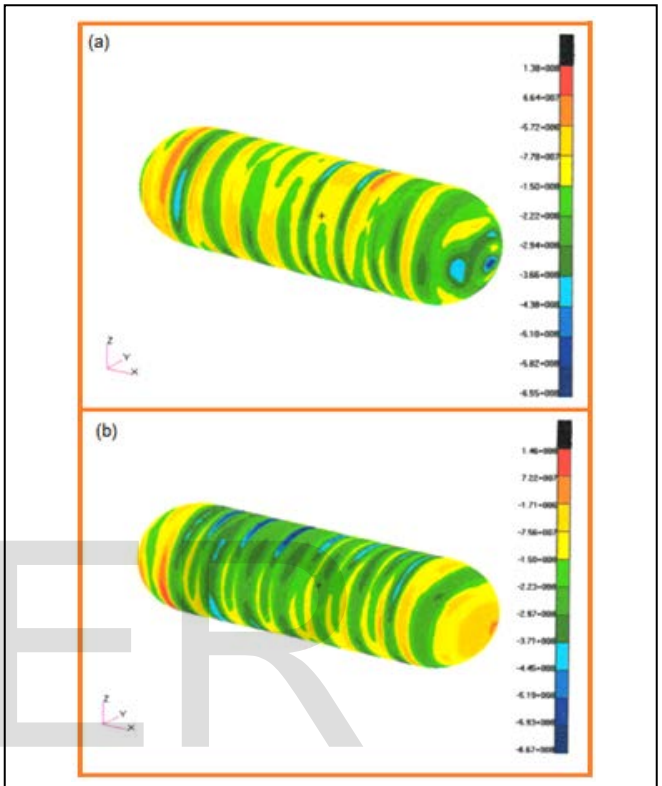

Fig. 10. Compressive stresses of submerged hull at SF = 0.45 (a) longitudinal and (b) circumferential.

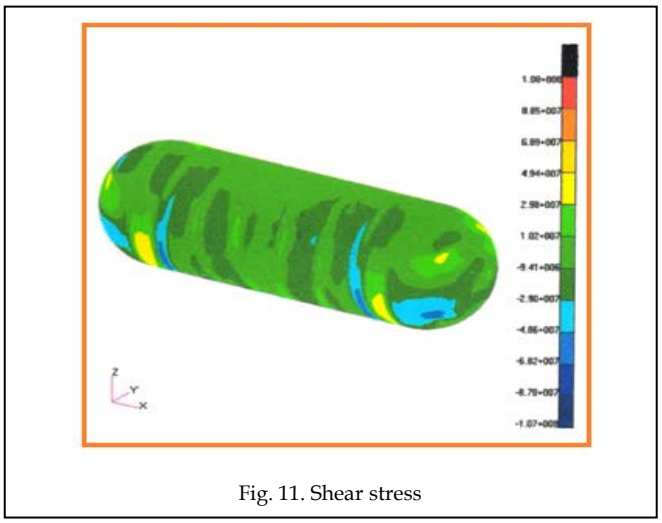

Fig. 11. Shear stress

4.3 Failure Analysis of Submersible Hull

The failure of the submersible hull was analyzed using Tsai-Hill criteria. The failure was assessed through the failure index. If the failure index reaches unity, then the mate-

rial is said to be failed. The failure indices of the submersible hull are given in table 2. The submersible hull failed when the explosion charge weight reached 25 kg.

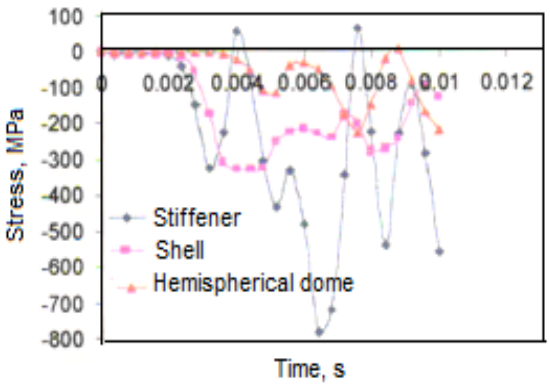

Fig. 12. Longitudinal stress-time history.

TABLE 2
FAILURE INDICES OF SUBMERSIBLE HULL

Charge weight (*W*), kg	Tsai-Hill criteria
1	0.0282
2	0.0550
5	0.0858
10	0.3267
15	0.6953
20	0.7897
25	1.0564

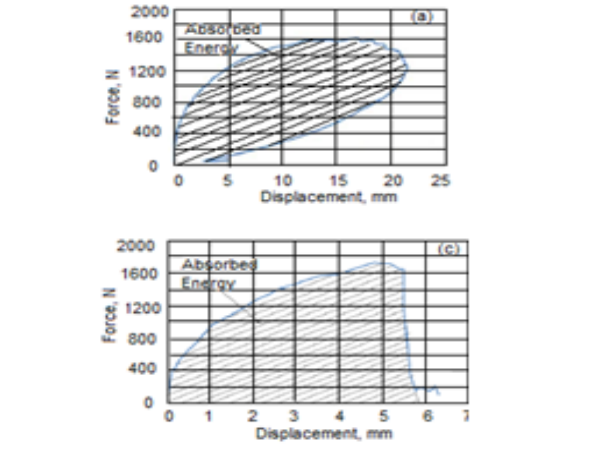

Fig. 13. Force-displacement curves of GFRP composites.

In order to confirm the failure results (obtained by the finite element analysis) of submersible hull due to shock loads, the impact test by falling weight was conducted experimentally on the E-glass/epoxy composite sheets. The force versus displacement graphs (figure 13a and 13b) show closed and open loops. The impact velocities were 2.5 m/s and 4.5 m/s for the specimens tested results of figure 13a and 13b, respectively. The area under the curve is the absorbed energy that is progressively transferred from the falling weight to the composite, when the saturation of the load carrying capacity of the plate is reached. The shaded areas represent for the energies absorbed by the specimens during impact tests resulting in closed type curves. For the rebounded specimens i.e. having closed type curves, the absorbed energy was calculated from the initial kinetic energy minus the rebound kinetic energy using the initial and rebound velocities. When the saturation of the load carrying capacity of the plate was reached, the perforation took place resulting damage in the composite. This phenomenon is observed with the open loop in figure 13b.

The damage extent at both front (impacted side) and back side of the specimens are depicted in figure 14. When the specimen was tested with a velocity of 2.5 m/s with falling height of 500 mm, no damage was observed in the specimen as depicted in figure 14a and 14b. When the specimen was tested with a velocity of 5.0 m/s with falling height of 500mm, the damage was observed in the specimen as illustrated in figure 14c and 14d.The impact energy was about 8.0 J. This can be correlated with the damage in the submersible hull with shock factor of 0.45 for the explosion charge weight of 25 kg.

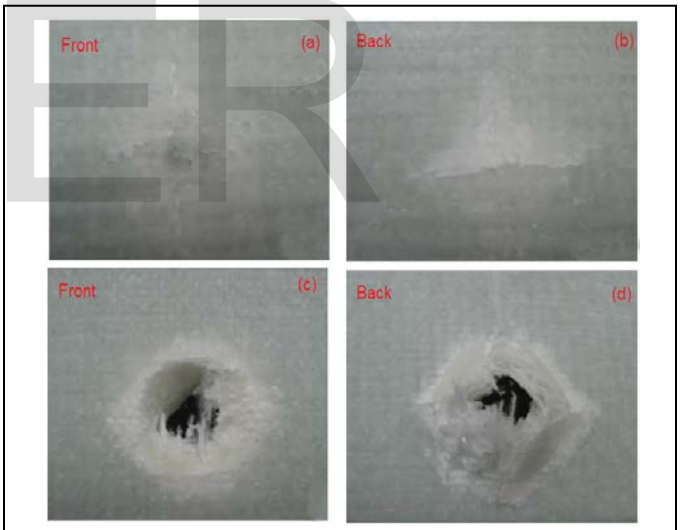

Fig. 14. Damages in the GFRP specimens.

5. CONCLUSIONS

The maximum displacement of the submerged hull has been found to be 0.0712 m for the explosion charge weight of 25 kg. The maximum tensile stress along the longitudinal direction of the submersible hull was 212 MPa which exceeded the yield strength of the material due to failure of fibers. The maximum shear stress exceeded 108 MPa in the submersible hull indicating the failure of matrix. The impact test by falling weight results are in good correlation with the results obtained through finite element analysis.

REFERENCES

[1] Australian Navy MK 46 Torpedo Test, 1999.
[2] H. Huang and K.C. Kiddy, "Transient interaction of a spherical shell with an underwater explosion shock wave and subsequent pulsating bubble," Shock and Vibration, vol.2, pp.451–460, 1995.
[3] Y.W. Kwon, and P.K. Fox, "Underwater shock response of a cylinder subjected to a side-on explosion," Journal of Computers and Structures, vol. 48, no.4, pp.637–646, 1993.
[4] Y.S. Shin and J.E. Chisum, "Modeling and simulation of underwater shock problems using a coupled Lagrangian-Eulerian analysis approach, "Shock and Vibration, vol.4, pp.1–10, 1997.
[5] J.M Santiago, M.H. Klaus and H.L. Wisniewski, "Finite element dynamic analysis of blast loaded cylinder," ASME proceedings, Conference on pressure vessel and piping and exhibition, pp.1-9, 1986.
[6] J. Jiang and M.D. Olson, "Nonlinear dynamic analysis of blast loaded cylindrical shell structures," Journal of Computers and Structures, vol.41, pp.41-52, 1991.
[7] S.W. Gong, and K.Y. Lam, "Transient response of stiffened composite submersible hull subjected to underwater explosive shock," Journal of Computers and Structures, vol.41, pp.27-37, 1998.
[8] B. Kotiveerachari and A.C. Reddy, "Interfacial effect on the fracture mechanism in GFRP composites," CEMILAC Conference, Ministry of Defence, India, 1 (b), pp.85-87, 1999.
[9] A. Chenaakesava Reddy, "Evaluation of curing process for carbon-epoxy composites by mechanical characterization for re-entry vehicle structure," International Journal of Scientific and Engineering Research, vol.6, no.3, pp.65-70, 2015.
[10] A. Chennakesava Reddy, "Evaluation of curing process for Kevlar 49-epoxy composites by mechanical characterization designed for brake liners," International Journal of Science and Research, vol.4, no.4, pp.2365-2371, 2015.
[11] A. Chennakesava Reddy, "Evaluation of curing process for bi-directional S-glass (5HS)/epoxy (780E +782H) composites fabricated by vacuum infusion process for wind energy blades," International Journal of Advanced Research, vol.3, no.4, pp.667-675, 2015.
[12] R.H. Cole, "Underwater Explosions," Princeton University Press, Princeton, 1948.
[13] Chennakesava R. Alavala. "Finite element methods: Basic concepts and applications," PHI Learning Pvt. Ltd., New Delhi, 2008.
[14] L.V.Al'tshuler, S.A. Novikov and I.I. Divnov, "Relationship between critical fracture stress time under explosive loading of metals," Doklady Akademii Nauk (USSR), vol.166, no.1, pp.67-70, 1966.